Supplement of Atmos. Chem. Phys., 23, 877–894, 2023
https://doi.org/10.5194/acp-23-877-2023-supplement

Atmospheric Chemistry and Physics
Open Access
EGU

Supplement of

Hemispheric-wide climate response to regional COVID-19-related aerosol emission reductions: the prominent role of atmospheric circulation adjustments

Nora L. S. Fahrenbach and Massimo A. Bollasina

Correspondence to: Nora L. S. Fahrenbach (n.l.s.fahrenbach@sms.ed.ac.uk)

Table S1. List of PDRMIP models and their main model characteristics. Table adapted from Myhre et al. (2017).

Model name	Resolution [a]	Aerosol setting	Aerosol processes
CanESM2	2.8°×2.8°, L35	Emissions	Full microphysics for aerosol-cloud interactions
CESM1-CAM4	2.5°×1.9°, L26	Fixed concentrations	No aerosol microphysics effects
CESM1-CAM5 [x]	2.5°×1.9°, L30	Emissions	Full aerosol microphysics
ECHAM6.3	1.9°×1.9°, L47	Emissions	Full aerosol microphysics
GISS-E2-R [x]	2.0°×2.5°, L40	Fixed concentrations	No aerosol microphysics effects
HadGEM2-ES	1.9°×1.3°, L38	Emissions	Full microphysics for aerosol-cloud interactions
HadGEM3-GA4 [x]	1.9°×1.3°, L85	Fixed concentrations	Microphysics for aerosol-cloud interactions (not for BC and dust)
IPSL-CM5A [x]	3.8°×1.9°, L39	Fixed concentration	Aerosol microphysics for Twomey effect
MPI-ESM	1.4°×1.4°, L47	Climatology year 2000	No aerosol chemistry (no aerosol experiments performed)
NorESM1-M [x]	2.5°×1.9°, L26	Fixed concentrations	Microphysics of aerosol-cloud interactions included through prescribed cloud condensation nuclei
MIROC-SPRINTARS [x]	1.4°×1.4°, L40	HTAP2 emissions	Full microphysics for aerosol-cloud interactions

[a] "L" denotes number of vertical levels

[x] Models which performed the BCx10a and SULx10a simulations with a fully coupled atmosphere-ocean and were considered in this study

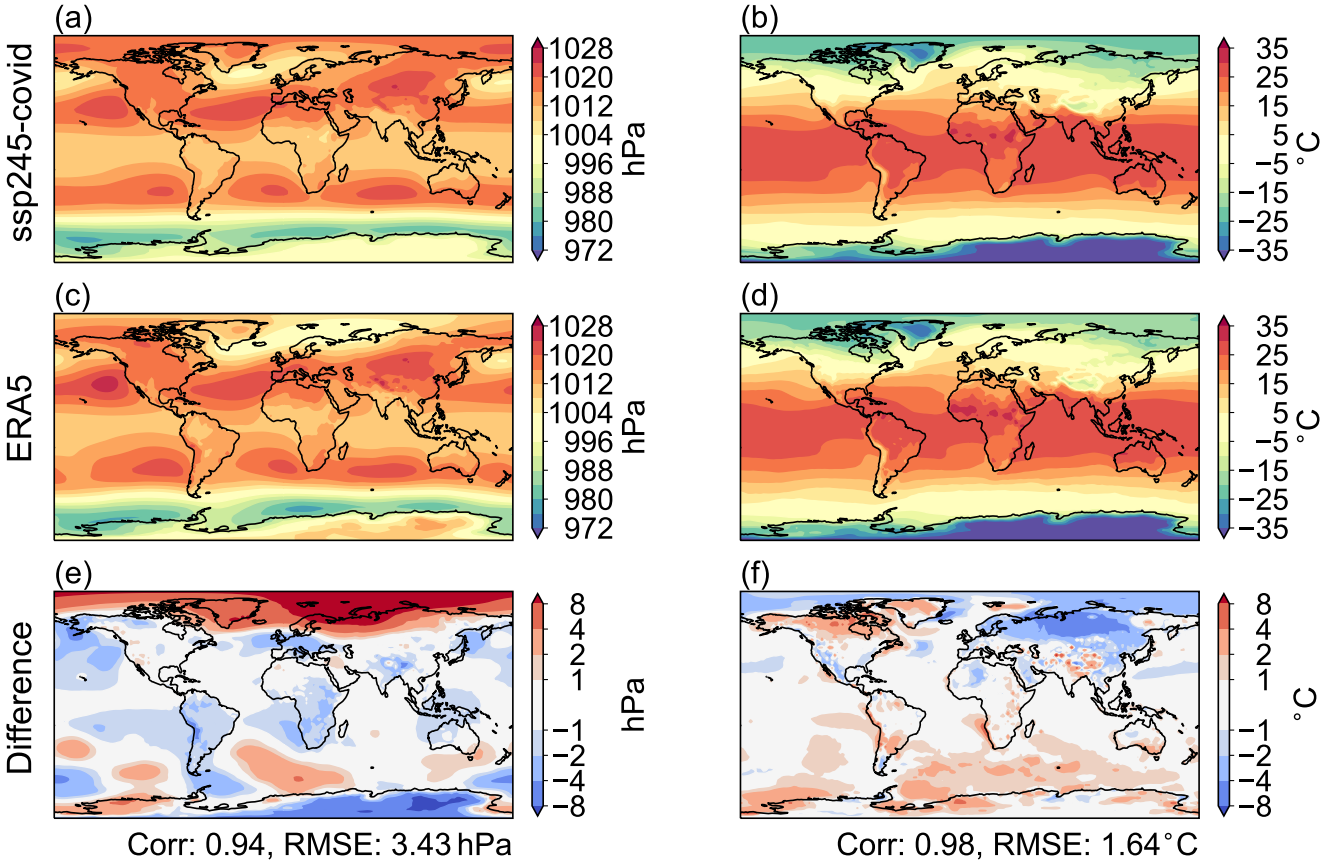

Figure S1. Comparison between spatial patterns in (a, c, e) sea-level pressure and (b, d, f) near-surface air temperature for JFMAM 2020 from ssp245-covid simulations and ERA5 reanalysis data as well as their difference (ssp245-covid minus ERA5). The spatial correlation coefficient coefficient (corr) and global root mean square error (RMSE) are given.

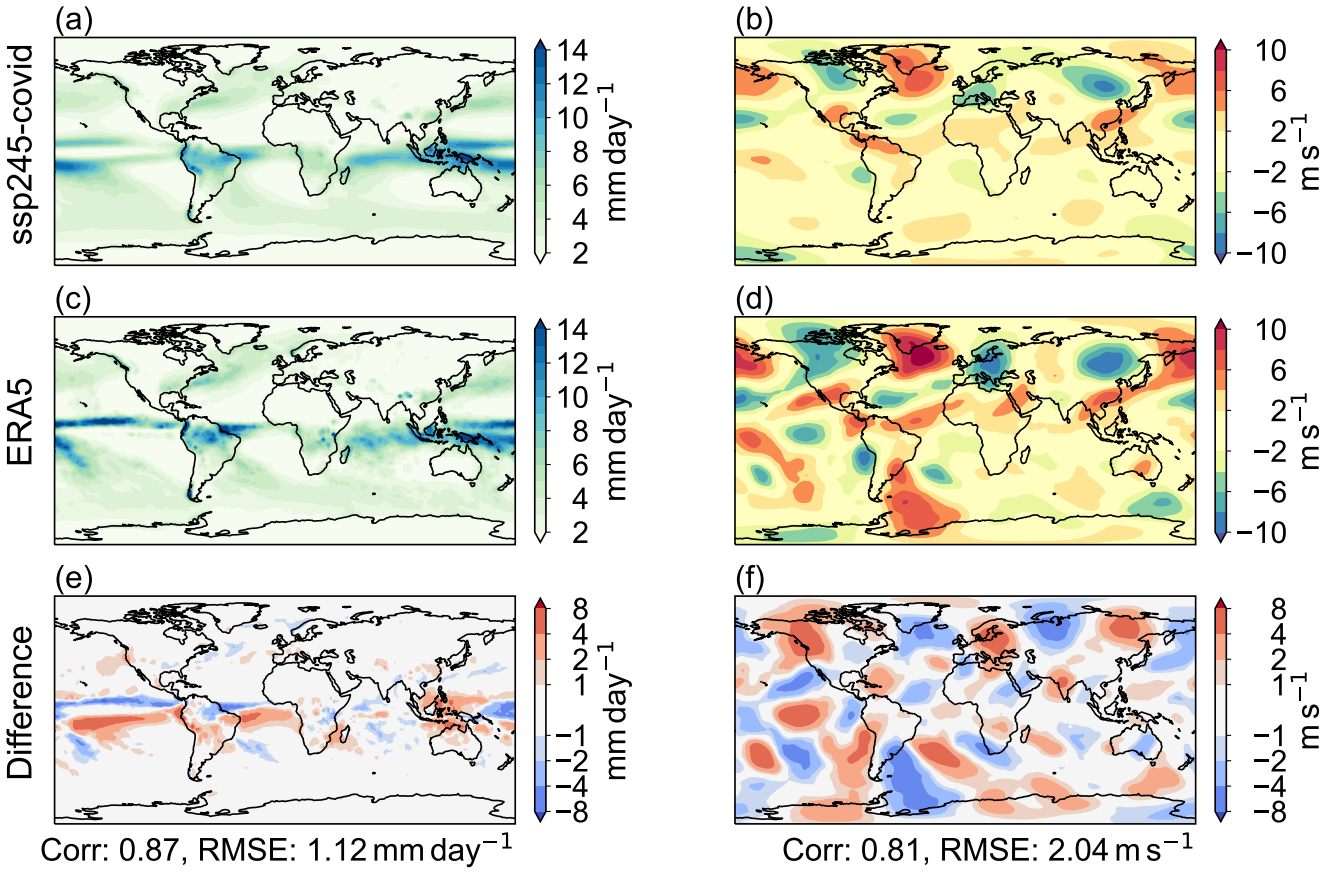

Figure S2. Comparison between spatial patterns in (a, c, e) precipitation rates and (b, d, f) meridional wind speed for JFMAM 2020 from ssp245-covid simulations and ERA5 reanalysis data as well as their difference (ssp245-covid minus ERA5). The spatial correlation coefficient coefficient (corr) and global root mean square error (RMSE) are given.

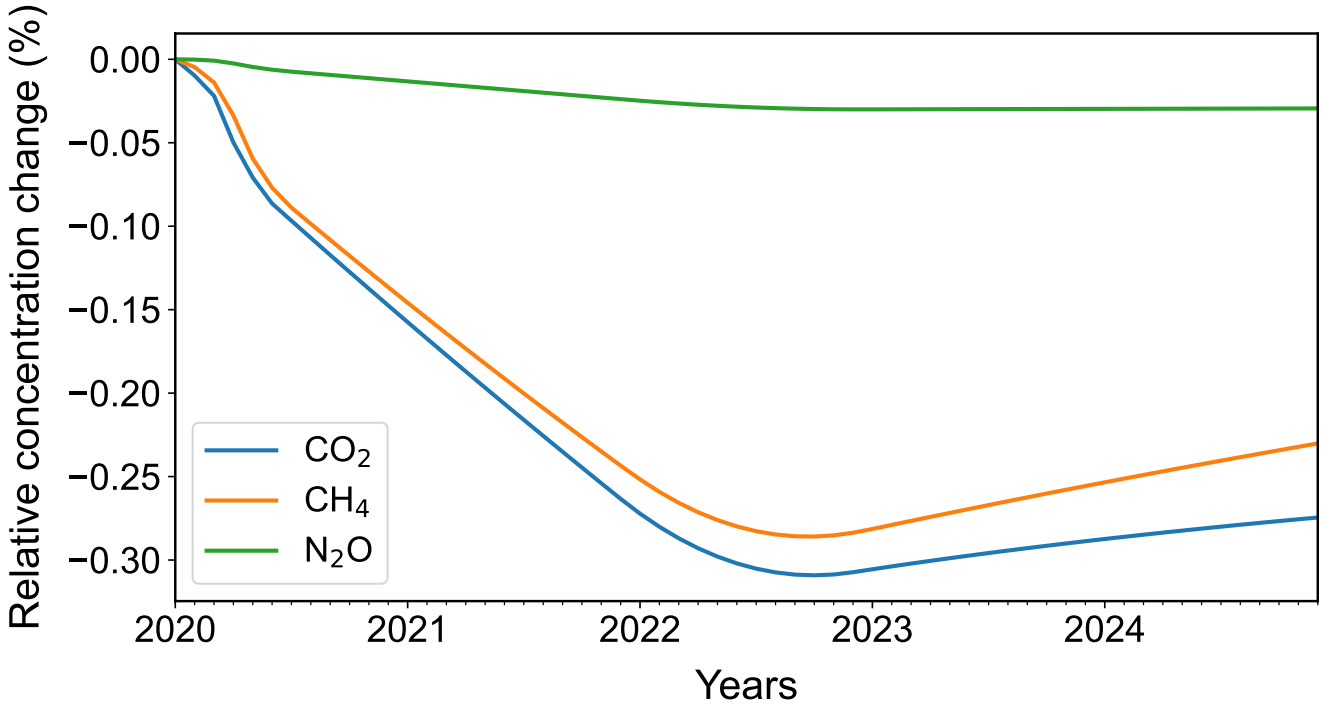

Figure S3. Relative change in global greenhouse gas concentrations of CO_2, CH_4 and N_2O between the ssp245-covid and baseline simulations from 2020 to 2025. GHGs concentrations for the ssp245-covid runs were reconstructed based on mobility data.

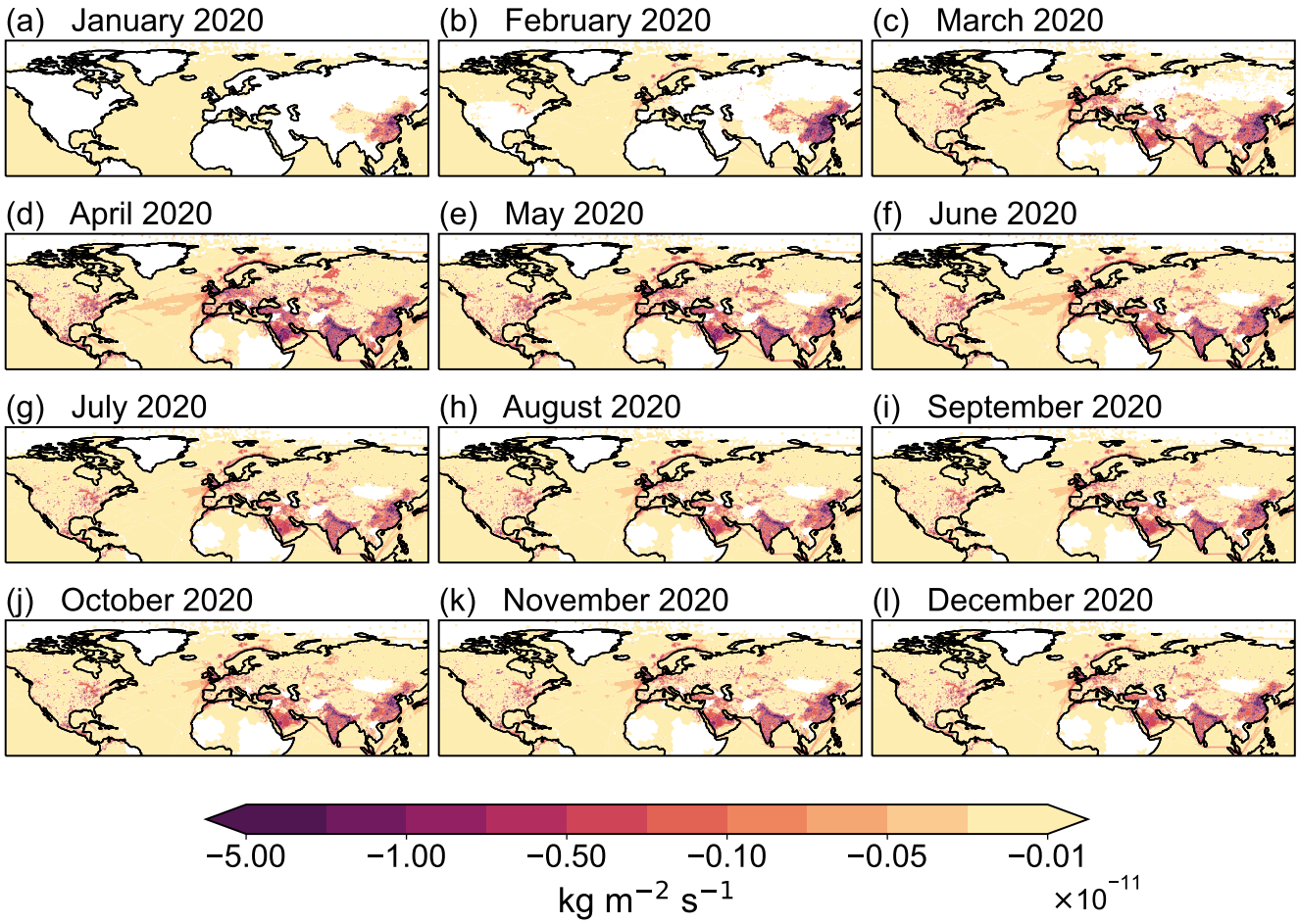

Figure S4. Changes in monthly SO_2 emissions over the Northern Hemisphere during 2020. White regions indicate that the change in emission is zero (often related to emissions being zero originally) or increased.

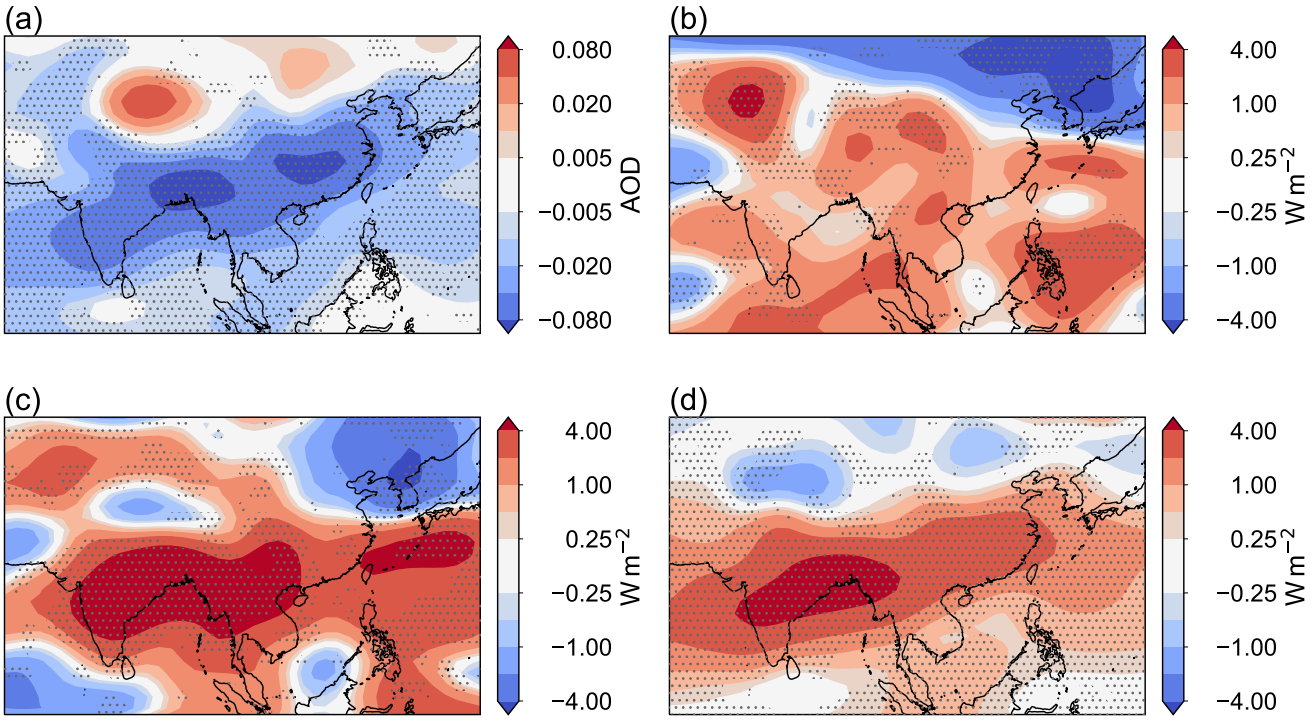

Figure S5. Spatial patterns of MEM anomalies in (a) AOD at 550 nm, (b) all-sky net top-of-atmosphere (TOA) SW radiation, (c) all-sky surface downwelling SW radiation and (d) clear-sky surface downwelling SW radiation for MAM 2020. Stippling indicates where at least 70% of the models agree on the sign of change.

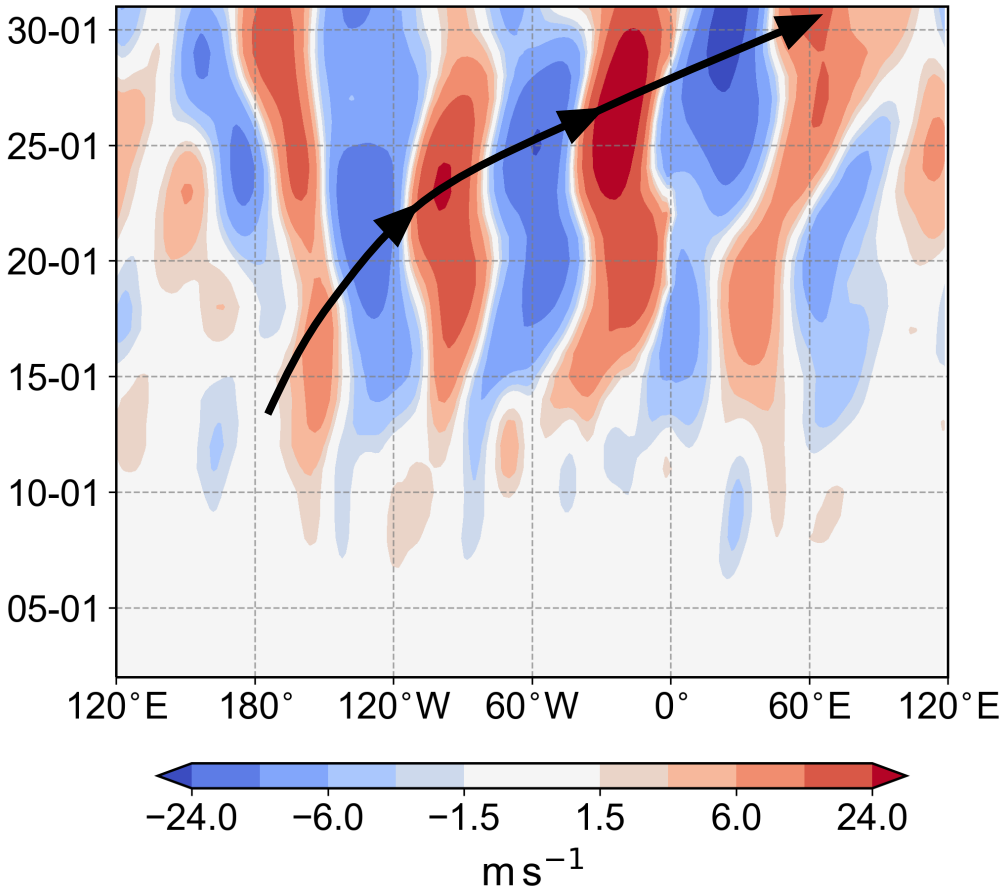

Figure S6. Hovmoller visualisation of the MPI-ESM1-2-LR anomalies in 250 hPa-meridional wind speed averaged between 30° N and 60° N for January 2020 and using a 5-day centred, unweighted rolling mean. The black arrow shows the suggested path of the Rossby wave train.

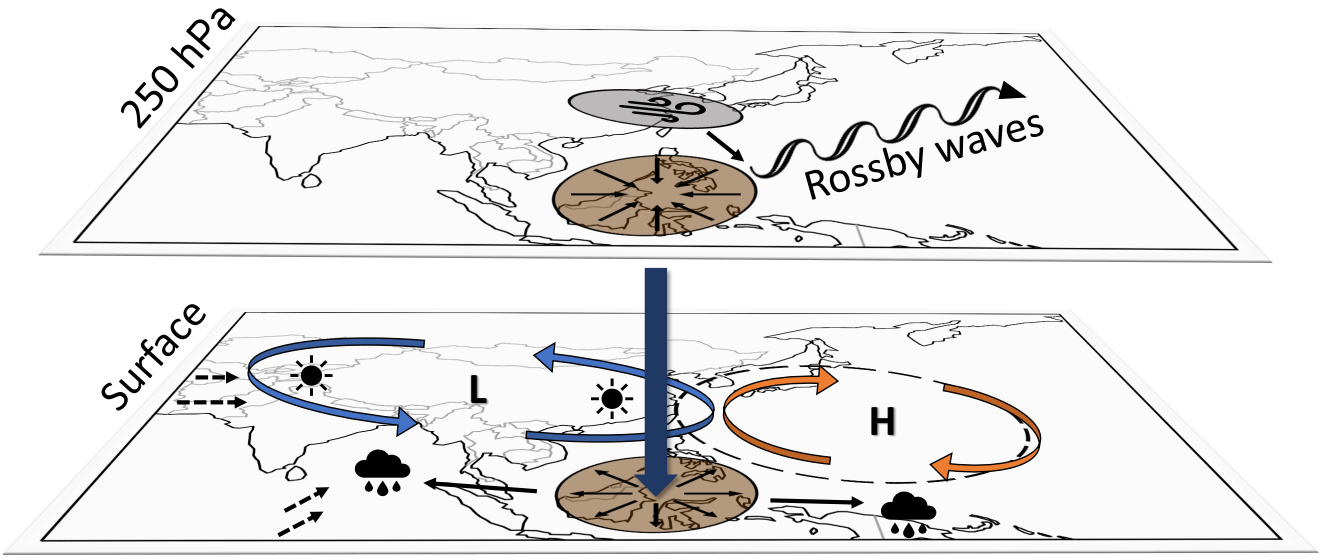

Figure S7. Schematic of the generation of Rossby waves associated with the reduction of aerosol emissions over India and eastern China in MAM 2020. The dark blue arrow represents vertical descending motion and the curved blue and orange arrows show low-pressure and high-pressure anomalies, respectively. Centres of divergence and convergence are shown as brown circles and the associated circulation with black arrows. Westerly winds over the Indian Subcontinent and southwesterly winds over the Indian Ocean are shown as dashed arrows. The East Asian jet core is indicated by a grey ellipse and the climatological extend of the western Pacific subtropical high by a dashed ellipse.

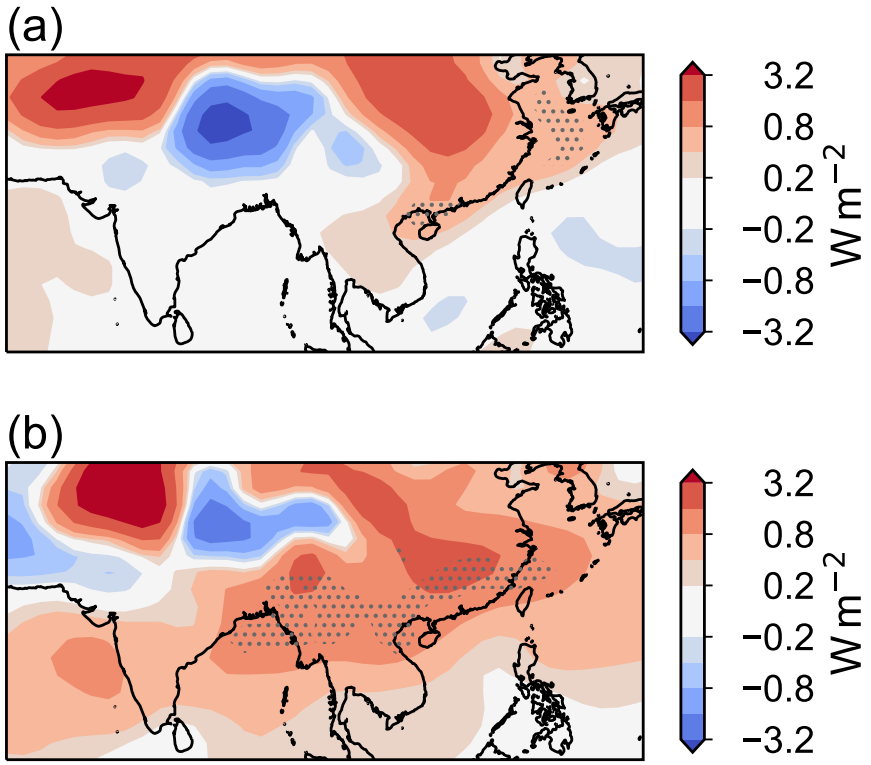

Figure S8. Spatial patterns of MEM anomalies in net clear-sky radiation at the top of the atmosphere for (a) JF and (b) MAM 2020. Stippling indicates where the ratio of the CovidMIP anomalies to the standard deviation in the pre-industrial simulations exceeds the value of one.

References

Myhre, G., Forster, P. M., Samset, B. H., Hodnebrog, O., Sillmann, J., Aalbergsjo, S. G., Andrews, T., Boucher, O., Faluvegi, G., Flaeschner, D., Iversen, T., Kasoar, M., Kharin, V., Kirkevag, A., Lamarque, J.-F., Olivie, D., Richardson, T. B., Shindell, D., Shine, K. P., Stjern, C. W., Takemura, T., Voulgarakis, A., and Zwiers, F.: PDRMIP: A Precipitation Driver and Response Model Intercomparison Project - Protocol and preliminary results, Bull. Amer. Meteor. Soc., 98, 1185–1198, https://doi.org/10.1175/BAMS-D-16-0019.1, 2017.